

Texture and stress in nickel layers with incorporated zirconia particles

P. Angerer^{1,*}, P. Pessenda-Garcia¹, E. Neubauer²,
G. E. Nauer¹

¹ECHEM Kompetenzzentrum für angewandte Elektrochemie GmbH, Viktor-Kaplan-Straße 2, A-2700 Wiener Neustadt, Austria

²ARC Seibersdorf research, A-2444 Seibersdorf, Austria

* Contact author; e-mail: paul.angerer@echem.at

Keywords: texture, stress, powder diffraction, nickel layers, zirconia

Abstract. Nickel layers provided for tribological applications with a thickness between 30 and 150 μm were deposited electrochemically on steel substrates using zirconia nanoparticles as reinforcement material. The aqueous electrolyte containing nickel sulphate, nickel chloride, and boric acid was used and nickel platelets were used as anodes. The content of the zirconia was up to 5 wt.%. The morphology of pure nickel and nickel-zirconia layers were analysed by scanning electron microscopy (SEM) and by focused ion beam (FIB) technique. A significant reduction of the grain size as an effect of the zirconia incorporation has been found. This was confirmed by XRD investigations. For the subsequent texture determination, the pole figures of the nickel Bragg reflections (111), (200) and (311) were measured. Two basic types of texture were found, texture type I, a fibre texture in [100] direction and texture type II, also a fibre texture. In very few samples a combination of both of these texture types was observed. The zirconia particle addition reduces the prominence of the texture significantly. Finally deformation (strain) and residual stress determinations using the $\sin^2\psi$ method (χ -mode, axis of sample rotation perpendicular to ω - and 2θ -axis) have also been undertaken.

Introduction

Currently the production of composite materials is of increasing interest. The main advantage of such materials is the possibility to improve a specific property in a precise and controllable manner due to the incorporation of particles. Unique functional properties of composite coatings are derived from the presence of particles dispersed in a metallic matrix and/or from the exposed particles which are only partly engulfed at the coating surface [1,2]. The properties of the composite coatings depend on the interaction of particles within the metal matrix, and ideally combine the advantages of the two materials. The development of composite coating technology has progressed so far that applications can now be found in general consumer products [3,4], with more applications related to microelectronics, micromechanical

systems and precision engineering [5]. Investigations on the texture of Ni layers with incorporated silicon carbide particles were recently published [6]. The envisaged application of the nickel layer samples studied in this work comprehends the area of tribology. The investigation of the influence of applied current density, temperature and pH of the electrolyte solution on the microstructure was an issue of this study.

Experimental methods

Synthesis of the samples

Nickel based composite layers were deposited from a Watts bath using ZrO_2 nanoparticles as reinforcement material. The electrolyte was a nickel Watts bath containing 300 g/l $\text{NiSO}_4 \cdot 6\text{H}_2\text{O}$ (Fluka, $\geq 99\%$), 40 g/l $\text{NiCl}_2 \cdot 6\text{H}_2\text{O}$ (Alfa Aesar, $\geq 99.3\%$), 40 g/l H_3BO_3 (Fluka, $\geq 99.5\%$). Two types of ZrO_2 nanoparticles with a particle size of 5 nm (produced in ARCS by a sol-gel process) and 40 nm (commercial particles) were used. The pH was adjusted using either NaOH or H_2SO_4 . Nickel platelets (Alfa Aesar, $\geq 99.5\%$) were used as anodes and polished steel cathodes as substrates. For all the experiments reported in this paper the same electrochemical cell geometry was used. The electrolyte was agitated with a magnetic stirrer. All depositions were done galvanostatically using a pulse reverse rectifier (Plating Electronic). The 40 nm zirconia powder was used for most of the experiments.

Characterization

The surface of the samples was characterized by scanning electron microscopy (ESEM Quanta 200 3D, FEI) and cross sections were prepared by focused ion beam (FIB) technique.

Texture and stress determination

The X-ray investigations (X'Pert powder diffractometer in combination with automatic texture cradle PW3068/00 ATC3, Philips, NL) were performed using $\text{CuK}\alpha$ radiation (40kV, 30 mA). Diffractograms were measured in Bragg-Brentano geometry using a step size of 0.05° in 2θ and a counting time of 1 s/step. The pole figure measurements were performed using incremental rotation steps in pole distance ψ of 5° and in azimuth φ also of 5° , resulting in 1296 measuring points (counting time of 5 s to 10 s each according to the intensity of the corresponding diffraction peak. For the stress determination the Bragg reflection (3 1 1) was selected. The intensity for the corresponding angle between 91° and 95° 2θ was scanned. The step size was 0.05° in 2θ (counting time 20 s/step). The stress measurements were performed using the χ -mode, i.e. the angle of sample rotation was perpendicular to the ω - and to the 2θ -axis. The sample tilt angles were selected in a way to achieve an equidistant sequence of $\sin^2\psi$. The maximum tilt angle ψ was 75° . Each series ($\psi = 0^\circ, \pm 23.2^\circ, \pm 33.9^\circ, \pm 43.1^\circ, \pm 52.1^\circ, \pm 61.9^\circ$, and $\pm 75.0^\circ$) was repeated for three different azimuthal angles ($\varphi = 0^\circ, 45^\circ$, and 90°), therefore for each sample 39 scans have to be measured. The exact peak position was obtained by least square refinement methods assuming a pseudo-Voigt function of the diffraction maximum (program PC-APD, Philips Analytical). For the calculation of the strain the precise peak position of a stress-free standard sample has to be determined. A nickel powder was embedded as a reference sample in an epoxy resin. The surface was subsequently polished. The position of the Bragg reflection (3 1 1) of this reference was similarly measured up to a tilt angle of 75° . In a diagram $\theta(\psi)$ (reference) versus $\sin^2\psi$, a value for θ_0

$= \theta(\psi=0)$ was calculated by linear regression. The variation of $\theta(\psi)$ in the reference sample was very small.

Results

FIB scanning electron microscopy

The SEM-FIB investigations showed that the samples with zirconia particles showed a significantly finer grain structure. Generally, an inhomogeneous grain structure has been found (confer figure 1). The ion etching sample preparation technique revealed that the regions with finer grains are related with a higher concentration of incorporated zirconia particles.

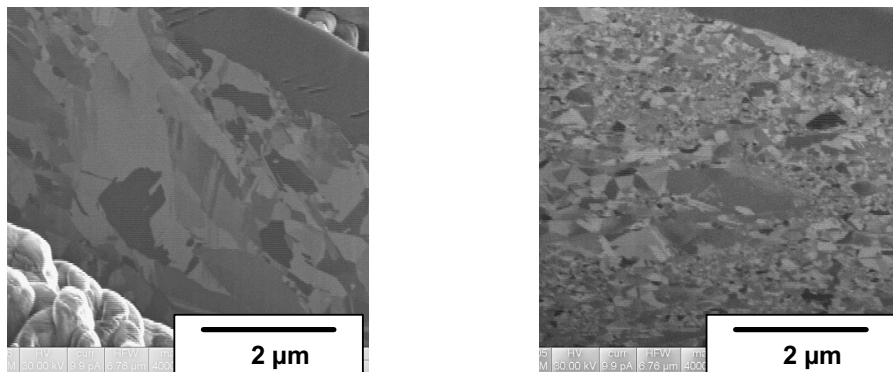


Figure 1. SEM-FIB micrographs of cross-sections of Ni-layer samples: nickel layer without zirconia particles (left), sample with incorporated zirconia particles (right).

Texture and stress determination

Conventional X-ray diffraction studies (Bragg-Brentano-geometry) already showed a very strong change of the intensities of the diffraction peaks. The relative intensity of the diffraction peak 200 varies by 1-2 orders of magnitude.

A pole figure is defined as the two-dimensional distribution function of the normal direction of a specific lattice plane. The determination of several pole figures of the nickel diffraction peaks 111, 200, and 311 showed that the layer samples can be divided into two different texture types: type I (confer the pole figures in figure 2) displays annular maxima which indicates a fibre texture. The corresponding tilt angle (angle between direct lattice directions 111 and 100: 54.7° and 311 and 100 25.2° , respectively) indicates a fibre direction in 100 direction. Texture type II (pole figures also in figure 2) is also related with annular maxima. This suggests clearly a fibre texture. However, an exact determination was not possible in this case. Most likely a combination of different texture varieties is present. A fraction of the crystallites is orientated in 211 direction, which is in accordance with [6], where the influence of SiC particles in Ni layers has been studied. The prominence of the texture varies strongly between the samples.

The incorporation of zirconia coincides with a weaker texture development. Furthermore the formation of texture type II is enhanced. The diagram in figure 3 (left) displays crystallite

size plotted as a function of layer thickness. The symbols indicate the corresponding texture type. A smaller layer thickness and a smaller crystallite size are correlated with texture type II.

In the investigated nickel layer samples the variation of $\theta(\psi)$ as a function of the azimuthal angle φ was very small due to the isotropic character of the stress in the samples (cylindric symmetry of the stress tensor). Therefore a mean value

$$\theta(\psi) = \frac{1}{3} \cdot [\theta(\varphi = 0^\circ, \psi) + \theta(\varphi = 45^\circ, \psi) + \theta(\varphi = 90^\circ, \psi)] \quad (1)$$

was calculated. For the further analysis this value was used. For each specific sample orientation in ψ a corresponding strain value $\varepsilon(\psi)$ was then calculated according to the relation:

$$\varepsilon(\psi) = \frac{d(\psi) - d_0}{d_0} = \frac{\sin \theta_0}{\sin \theta(\psi)} - 1 \quad (2)$$

whereby $d(\psi)$ refers to the interplanar spacing at a specific tilt angle, d_0 indicates the interplanar spacing of the stress-free reference sample, $\theta(\psi)$ denotes the diffraction angle as a function of $\theta(\psi)$ and θ_0 refers to the diffraction angle of the reference sample obtained as described above.

The subsequent calculation of the residual stress in the samples was conducted using the principal relation describing a stress state with cylindrical symmetry:

$$\varepsilon(\psi) = \frac{1+\nu}{E} \cdot (\sigma_{11} - \sigma_{33}) \cdot \sin^2 \psi + \frac{1}{E} \cdot (\sigma_{33} - 2\nu \cdot \sigma_{11}) \quad (3)$$

whereby $E = 200$ GPa refers to the Young's modulus, and $\nu = 0.31$ refers to the Poisson's ratio of nickel metal. This equation can be simplified provided that in a thin layer no stress component perpendicular to the surface can exist ($\sigma_{33} = 0$, σ_{11} denotes the stress component parallel to the layer plane). In a diagram $\varepsilon(\psi)$ versus $\sin^2 \psi$ the slope equates then to $(1 + \nu) / E \cdot \sigma_{11}$ and the axis intercept to $-1 / E \cdot 2\nu \cdot \sigma_{11}$. This calculation has to be repeated for each measured layer sample. Further details relevant for the stress analysis of thin films by X-ray diffraction methods in general are given in [7].

The crystallite size determination was conducted using Scherrer's formula in the form:

$$d = \frac{K \cdot \lambda}{B - b} \cdot \cos \theta \quad (4)$$

where d denotes the average crystallite size, K is the shape factor (normally between 0.9 and 1), $\lambda = 1.54056$ Å, is the wavelength of the used copper $K\alpha$ radiation, B is the peak width (FWHM or integral breadth), $b = 0.08^\circ 2\theta$ is the instrumental standard profile width and θ denotes the diffracting angle of the given peak. For the determination of d the nickel diffraction peak at $2\theta = 93.0^\circ$ (3 1 1), was used. The peak breadth of three different azimuthal an-

gles ($\varphi = 0^\circ, 45^\circ$, and 90°) has been determined and an average value for the crystallite size was subsequently calculated (program PC-APD, Philips). These measurements are identical with the scans used for stress determination parameters at $\psi = 0$. The results correspond to the diffracting coherence length in the material. It is influenced by the real structure of the crystallites. Values obtained by SEM methods are larger by a factor of ~ 10 .

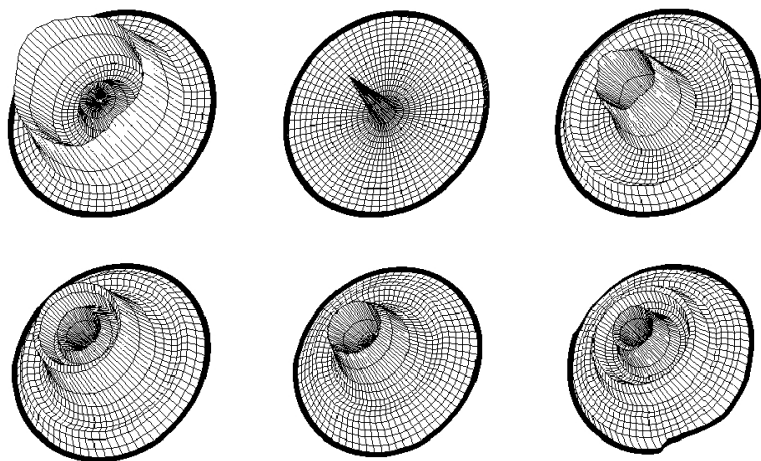


Figure 2. Pole figures of a sample with a strong pronounced texture: type I, fibre texture in 100 direction - pole figure (111) (top left) (200) (top middle), (311) (top right), type II, also fibre texture - pole figure (111) (bottom left) (200) (bottom middle), (311) (bottom right); the diffraction intensity is plotted as a function of pole distance and azimuthal angle (cylindrical coordinate system, mesh width of plotted grid 5°).

The stress determination as described above was performed routinely. The deviation of a linear behaviour in the $\sin^2\psi$ plot was most distinct in the strongly textured samples but small enough to justify the texture-free approach for this work. The results of the stress measurement are shown in figure 3 (right). A smaller crystallite size (obtained from X-ray diffraction data) is always related with higher residual stress values. Layer samples with smaller thickness show higher values for the residual stress. Samples with texture type I display a larger range of residual stress values (component σ_{11} between 0.10 and 0.40 GPa). The comparative values of samples with texture type II are between 0.22 and 0.37 GPa, respectively.

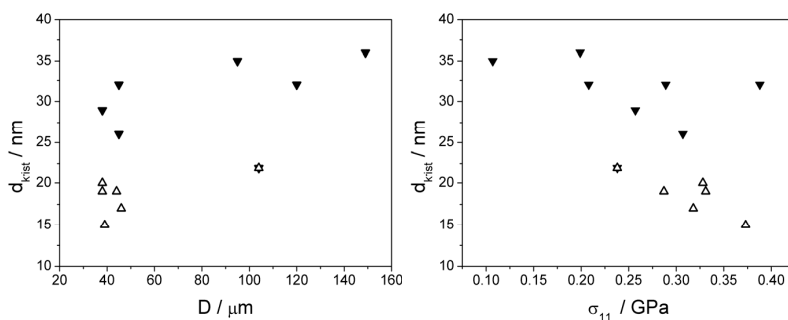


Figure 3. Results of the texture and stress determination: crystallite size plotted as a function of layer thickness (top), crystallite size plotted as a function of the residual stress (bottom); closed symbols refer to texture type I, open symbols refer to texture type II.

Concluding remarks

The incorporation of zirconia in the nickel layer samples influenced the microstructure of the material. The hardness of the material was increased. Furthermore the size of the nickel crystallites was reduced and the characteristic of the texture was reduced. The formation of texture type II is enhanced by the incorporated zirconia particles. Further investigations must be done to evaluate the effects with respect to the suitability of the material for potential tribological applications.

References

1. Hovestadt, A., Jansen, L. J. J., 1995, *J. Appl. Electrochemistry*, **25**, 519-527.
2. Broszeit, E., Heimke, G., Wiegand, H., 1971, *Metall*, **25**, 470.
3. Gyftou, P., Pavlatou, E.A., Spyrellis, N., Hatzilyberis, K.S., 2000, *Trans. Inst. Met. Finish.*, **78(6)**, 223.
4. Poeton, A.R., 1988, *Metals & Materials*, 4, 702-704.
5. Wielage, B., Steinhäuser, S., Lampke, T., Hofmann, U., Jakob, C., 2003, *Metall-oberfläche*, **57**, 25-28.
6. Pavlatou, E. A., Stroumbouli, M., Gyftou, P., & Spyrellis, N., 2006, *J. Appl. Electrochemistry*, **36**, 385-394.
7. Welzel, U., Ligot, J., Lamparter, P., Vermeulen, A.C., & Mittemeijer, E. J., 2005, *J. Appl. Cryst.*, **38**, 1-29.

Acknowledgements

This work was supported within the K plus programme by the Austrian Research Promotion Agency (Österreichische Forschungsförderungsgesellschaft, FFG) and the government of Lower Austria.